Highly bioavailable dust-borne iron delivered to the Southern Ocean during glacial periods

Elizabeth M. Shoenfelt[a,b,1], Gisela Winckler[a,b], Frank Lamy[c], Robert F. Anderson[a,b], and Benjamin C. Bostick[a]

[a]Lamont-Doherty Earth Observatory, Columbia University, Palisades, NY 10964; [b]Department of Earth and Environmental Sciences, Columbia University, New York, NY 10027; and [c]Alfred Wegener Institute, Helmholtz Centre for Polar and Marine Research, 27570 Bremerhaven, Germany

Edited by Edward A. Boyle, Massachusetts Institute of Technology, Cambridge, MA, and approved September 12, 2018 (received for review June 8, 2018)

Changes in bioavailable dust-borne iron (Fe) supply to the iron-limited Southern Ocean may influence climate by modulating phytoplankton growth and CO_2 fixation into organic matter that is exported to the deep ocean. The chemical form (speciation) of Fe impacts its bioavailability, and glacial weathering produces highly labile and bioavailable Fe minerals in modern dust sources. However, the speciation of dust-borne Fe reaching the iron-limited Southern Ocean on glacial–interglacial timescales is unknown, and its impact on the bioavailable iron supply over geologic time has not been quantified. Here we use X-ray absorption spectroscopy on subantarctic South Atlantic and South Pacific marine sediments to reconstruct dust-borne Fe speciation over the last glacial cycle, and determine the impact of glacial activity and glaciogenic dust sources on bioavailable Fe supply. We show that the Fe(II) content, as a percentage of total dust-borne Fe, increases from ∼5 to 10% in interglacial periods to ∼25 to 45% in glacial periods. Consequently, the highly bioavailable Fe(II) flux increases by a factor of ∼15 to 20 in glacial periods compared with the current interglacial, whereas the total Fe flux increases only by a factor of ∼3 to 5. The change in Fe speciation is dominated by primary Fe(II) silicates characteristic of glaciogenic dust. Our results suggest that glacial physical weathering increases the proportion of highly bioavailable Fe(II) in dust that reaches the subantarctic Southern Ocean in glacial periods, which represents a positive feedback between glacial activity and cold glacial temperatures.

iron speciation | Southern Ocean | iron bioavailability | dust | productivity

Iron (Fe) fertilization of phytoplankton in the Southern Ocean is thought to contribute to the glacial–interglacial changes in atmospheric CO_2 concentrations (e.g., refs. 1–6). Increased dust-borne Fe deposition and Fe fertilization of phytoplankton in the subantarctic South Atlantic Ocean is associated specifically with the latter half of CO_2 drawdown in the last glacial cycle, as evidenced by positive correlations between productivity proxies, nutrient utilization proxies, and dust/total Fe fluxes measured in marine sediment cores (1, 2, 6). Since John Martin made his Fe hypothesis in 1990 (7) through today, researchers have relied on total dust and total Fe fluxes to marine sediment cores in the Southern Ocean to evaluate the importance of Fe fertilization on geologic timescales (1, 2, 8, 9). The potential additional effect of the chemical form of dust-borne Fe is unknown, despite studies showing that glacial processes impact solid-phase Fe speciation and increase dust-borne Fe bioavailability in modern sources (10–12). Others have observed high dust-borne Fe solubility (13, 14) and high concentrations of leachable, bioavailable Fe^{2+} (15) in Antarctic ice cores at the Last Glacial Maximum (LGM) compared with interglacials, but these studies do not measure solid-phase dust-borne Fe speciation nor evaluate its impact on Fe solubility and bioavailability.

The solid-phase Fe in glaciogenic sediments is more labile and bioavailable than that in nonglaciogenic sediments because it comprises more Fe(II) versus Fe(III) minerals (10–12, 16). These Fe(II) minerals are typically primary Fe(II) silicates that are freshly weathered from bedrock, in contrast with secondary Fe(III) oxyhydroxides that have undergone more chemical weathering (10, 11). While glaciogenic sediments and glacial ice core dust have been shown to be highly efficient at fertilizing Fe-limited phytoplankton (10, 17), the impact of glaciogenic versus nonglaciogenic dust-borne Fe speciation on the bioavailable iron supply reaching the Southern Ocean over the last glacial cycle has not been quantified. Instead, all dust-borne Fe is considered equal in biogeochemical models, regardless of its solid-phase speciation (18, 19). In this paper, we use bulk Fe K-edge X-ray absorption spectroscopy (XAS) to determine the speciation—i.e., the average oxidation state [$Fe(II)/Fe_{total}$] and mineral composition—of dust-borne Fe deposited to Southern Ocean sediment cores over the last glacial cycle. We observe that $Fe(II)/Fe_{total}$ is higher in glacial versus interglacial periods, and that glacially derived primary Fe(II) silicates dominate the Fe deposited to the Southern Ocean during glacial periods. We use microprobe-based X-ray fluorescence (μXRF) and Fe K-edge XAS (μXAS) to confirm the presence of distinct, pure primary Fe(II) particles in the sediments that are physically weathered from bedrock and are not the result of diagenesis. Since previous work has shown that primary Fe(II) silicates are more bioavailable for a given Fe flux than other forms of Fe (10, 11), and the relationship between particulate Fe(II) and bioavailability is linear under Fe limitation (10), we show that primary Fe(II) flux is likely a better estimate of bioavailable Fe supply than dust flux or total Fe flux, and we propose a positive feedback between

Significance

Dust-borne iron fertilization of Southern Ocean phytoplankton contributes to lower glacial atmospheric CO_2. Previous studies evaluating the impact of dust on climate estimate bioavailable iron using total iron fluxes in sediment cores. Thus, all iron is considered equally bioavailable over geologic time, despite evidence that glaciers mobilize highly bioavailable iron from bedrock, which winds can deliver to the Southern Ocean. Here we reconstruct dust-borne iron speciation over the last glacial cycle, showing that highly bioavailable iron(II) silicate minerals are a greater fraction of total iron reaching the Southern Ocean during glacial periods. The abundance of iron(II) silicates likely controls the bioavailable iron supply to the Southern Ocean and contributes to the previously observed increase in glacial productivity and CO_2 drawdown.

Author contributions: E.M.S., G.W., and B.C.B. designed research; E.M.S., G.W., F.L., R.F.A., and B.C.B. performed research; E.M.S. and B.C.B. collected and analyzed spectra and microprobe maps; G.W. and F.L. developed the PS75/56-1 dust flux and Fe flux records; and E.M.S. wrote the paper with input from all authors.

The authors declare no conflict of interest.

This article is a PNAS Direct Submission.

Data deposition: All data have been deposited in the Columbia University Academic Commons, and are available at the persistent URL https://doi.org/10.7916/D8X07QHG.

[1]To whom correspondence should be addressed. Email: shoen@ldeo.columbia.edu.

This article contains supporting information online at www.pnas.org/lookup/suppl/doi:10.1073/pnas.1809755115/-/DCSupplemental.

Published online October 15, 2018.

glacial activity and cold glacial temperatures through Fe fertilization of the Fe-limited Southern Ocean.

Results and Discussion

Fe(II) Fluxes in the Subantarctic South Atlantic and South Pacific. Our solid-phase Fe speciation and bioavailability reconstructions are based on two sediment cores in the subantarctic Southern Ocean: TN057-06 [42.91°S, 8.9°E, 3,751 m water depth, the site survey core for Ocean Drilling Program (ODP) 1090 (20)] from the subantarctic South Atlantic (9) and PS75/56-1 (55.16°S, 114.79°W, 3,581 m water depth) from the subantarctic South Pacific (8) (*SI Appendix*, Fig. S1). All samples were obtained from 1-cm widths in the core and freeze-dried without further processing. These cores have both been used to show that Fe fluxes to the subantarctic Southern Ocean were ∼3 to 5 times higher in glacial versus interglacial periods, and to link high dust and Fe fluxes at the LGM to Fe fertilization of phytoplankton (1, 8, 9). In this paper, we use the ^{230}Th-normalized ^{232}Th flux as a proxy for terrestrial dust inputs (21, 22), and convert to dust flux using the average ^{232}Th content of upper continental crust (10.7 ppm) (23, 24) (Fig. 1*A*).

Representative bulk Fe K-edge XAS spectra (Fig. 1*C*) from South Atlantic core samples across the last glacial cycle (Fig. 1*A*) are distinctly different due to variable Fe(II)/Fe$_{total}$ (shown as percentages, Fig. 1*B*). Bulk XAS uses a typical X-ray beam size of 1 mm × 10 mm, and obtains the average Fe(II)/Fe$_{total}$ of a given sediment sample as a result (26). During glacial periods with high dust fluxes (Fig. 1*A*), positions of maximum absorption are ∼7,130 eV, which indicate high Fe(II) content (10) (Fig. 1*C*). In contrast, during interglacial periods with low dust fluxes (Fig. 1*A*), positions of maximum absorption are ∼7,133 eV, which indicate high Fe(III) content [and thus low Fe(II)] (10) (Fig. 1*C*).

We present paleorecords of Fe(II) flux through the last glacial cycle, based on XAS of our minimally processed marine sediment core samples from the subantarctic Atlantic and Pacific sectors of the Southern Ocean (Fig. 2). The Fe(II) flux reconstructions span the last 100,000 and 140,000 y for the South Atlantic and South Pacific, respectively (Fig. 2 *B* and *D*). The Fe(II)/Fe$_{total}$ values (Figs. 1*B* and 2 *A* and *C* and *SI Appendix*, Fig. S2) were determined using bulk Fe K-edge XAS and linear combination fitting (LCF) to find the combination of published standards with known Fe(II) content that best describes the spectral features (10) (see *Materials and Methods*). The Fe(II)/Fe$_{total}$ values were then multiplied by the ^{230}Th-normalized total Fe flux to create the Fe(II) flux (Fig. 2). Fe quantification for PS75/56-1 is detailed in *SI Appendix*, Fig. S3. The Fe(II)/Fe$_{total}$ is positively correlated with both dust flux and total Fe flux across the full range of data in both cores (correlation plots, R^2 values, and *P* values are shown in *SI Appendix*, Fig. S4), and the Fe(II)/Fe$_{total}$ was ∼6× higher at the LGM compared with the current interglacial period in both regions of the ocean (from ∼5 to ∼30% Fe(II)/Fe$_{total}$; Fig. 2 *A* and *C*). Edge position data were used to confirm the oxidation state information obtained by LCF (*SI Appendix*, Figs. S5 and S6). We also collected XAS spectra on wet (unprocessed), freeze-dried, and oven-dried sediments (50 °C overnight) all from TN057-06 at 90 cm to 91 cm depth (dated 25.47 ka), to test the impacts of sample handling on Fe speciation. All spectra, Fe(II) concentrations, and mineral compositions were the same (within error) for all treatments, suggesting Fe speciation in the sediments is not observably altered with typical sediment core sample preparation (*SI Appendix*, Fig. S7).

The Fe(II) content of dust-borne Fe reaching the Southern Ocean is higher in glacial periods than in interglacial periods. Thus, glacial dust sources contain more reduced Fe species than interglacial dust sources, which is likely the result of higher and lower glacial activity (10–12), respectively, in the source regions.

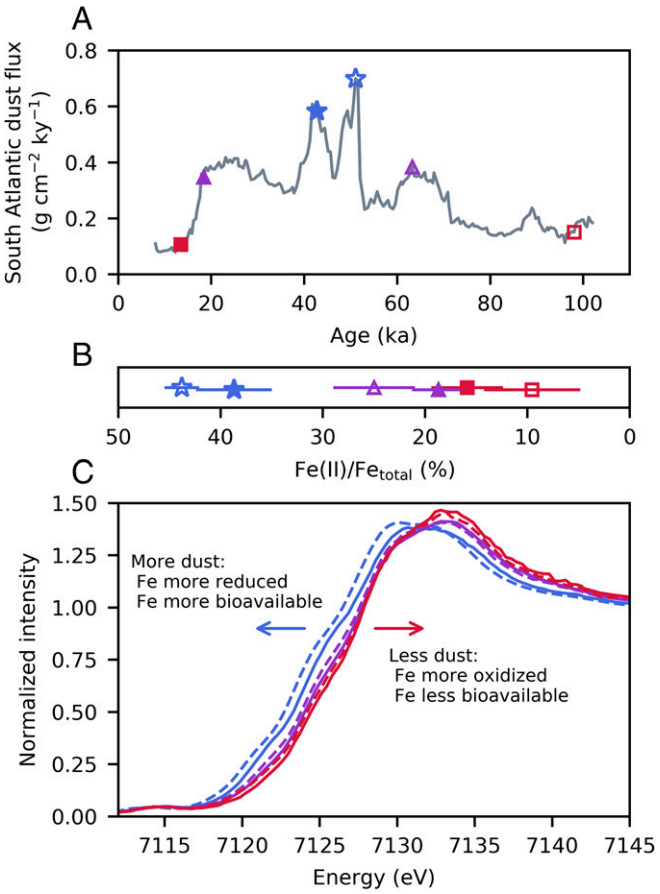

Fig. 1. (*A*) The ^{230}Th-normalized ^{232}Th-based dust flux (gray) from the South Atlantic marine sediment core (TN057-06) plotted with representative high (blue stars), medium (purple triangles), and low (red squares) dust flux samples. (*B*) Fe(II)/Fe$_{total}$ values for the representative samples calculated using LCF of the sample with mineral standards of known Fe(II) content, using the Fe K-edge k^3-weighted chi function. All error bars on Fe(II)/Fe$_{total}$ values are based on the goodness of fit and are produced using Larch (25). The colors and open and closed symbols in *A* match those in *B*. (*C*) Fe K-edge XAS spectra for the representative samples. Colors in *C* are the same as in *A* and *B*, with dashed lines corresponding to open symbols and solid lines corresponding to filled symbols. Lower edge positions indicate Fe that is more reduced and therefore more bioavailable, and vice versa (10). Possible ice-rafted debris and other terrestrial mineral contributions to the ^{230}Th-normalized ^{232}Th dust proxy are the topic of ongoing research, especially for the high peaks in Marine Isotope Stage 3 (blue stars).

Glaciogenic Primary Fe(II) Minerals Modulating Fe(II) Fluxes over Time. Primary Fe(II) silicate minerals (e.g., biotite and hornblende) represent the largest contributions to Fe(II)/Fe$_{total}$ and thus Fe(II) flux in glacial periods, as determined with bulk XAS (*SI Appendix*, Figs. S2 and S8). The spectra were fully described by a mix of crystalline mineral phases (e.g., biotite, hornblende) and more amorphous inorganic Fe (e.g., ferrihydrite). Our XAS method is sensitive to organic Fe species (30), but these were not observed.

The observed Fe(II)/Fe$_{total}$ and the contributions from Fe(II) silicates are both higher in glacial periods, and lower in interglacial periods. The primary Fe(II) silicate minerals that dominate glacial Fe fluxes are consistent with physical weathering/glacial activity, based on mineralogical studies of modern glaciogenic dust sources (10, 11). In previous work, we have shown that biotite and hornblende minerals in natural South American dust can alleviate Fe limitation when added as the sole Fe source in diatom cultures (10). The solubility (11), general lability, and direct bioavailability (10) of these minerals,

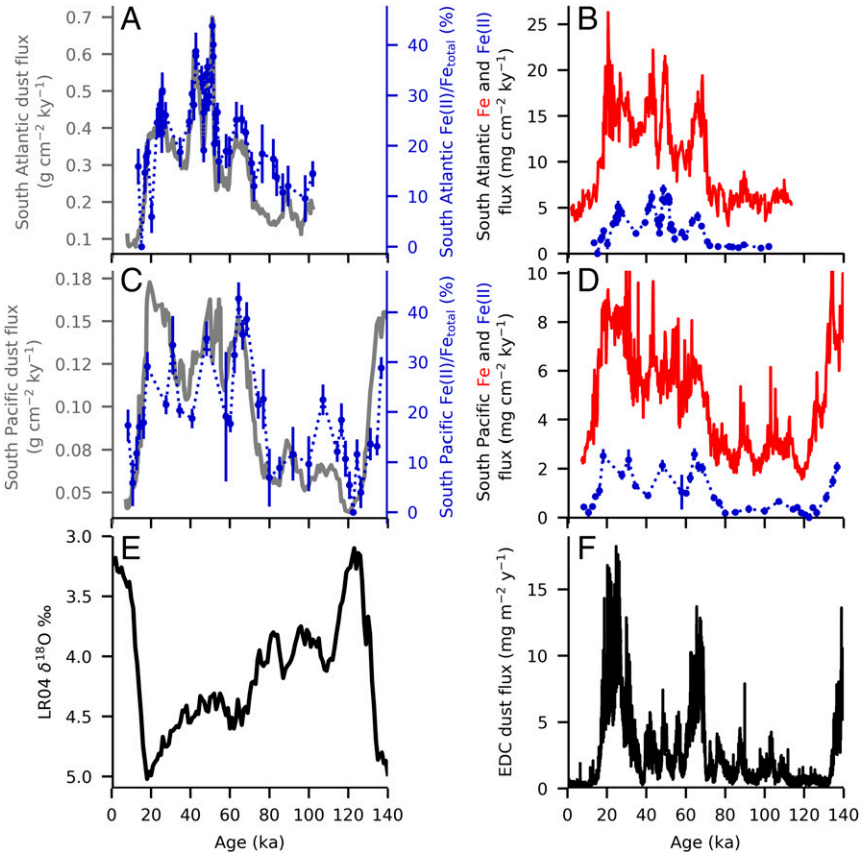

Fig. 2. (*A* and *C*) Dust fluxes and Fe(II)/Fe$_{total}$ records, with (*B* and *D*) total Fe fluxes and Fe(II) fluxes over the last glacial cycle for (*A* and *B*) the South Atlantic (TN057-06) and (*C* and *D*) the South Pacific (PS75/56-1). (*A* and *C*) Dust fluxes are represented with gray solid lines (gray axes). Fe(II)/Fe$_{total}$ records are blue circles connected with a dotted line (blue axes), and they are calculated the same way as those in Fig. 1*B*. The error bars for Fe(II)/Fe$_{total}$ are based on the goodness of fit using the best-fit combination of standards, and are produced using Larch (25). (*B* and *D*) Fe fluxes are ^{230}Th-normalized (red lines), and LCF-based Fe(II) fluxes (blue circles connected with a dotted line) are the Fe(II)/Fe$_{total}$ fraction multiplied by the Fe flux. The error bars for Fe(II) flux were calculated by propagating the errors on Fe(II)/Fe$_{total}$, Fe concentration, and ^{230}Th MAR. (*E*) The LR04 δ^{18}O benthic stack (27) (climate proxy) shows the glacial–interglacial cycle for the period of time spanned by the samples in this study. High δ^{18}O values indicate cold glacial climates, and vice versa (28). Note that the axis is inverted, by convention. (*F*) The mineral dust flux to the Antarctic EPICA Dome C (EDC) ice core shows trends in dust supply in this time period (29).

combined with their prevalence in modern glaciogenic dust sources (10), suggest that they are important to phytoplankton in the mixed layer of the ocean. Secondary Fe(II) minerals describe good portions of the low interglacial Fe(II) fluxes (*SI Appendix*, Fig. S8), which is consistent with chemical weathering processes that are more important in interglacial periods (31).

To confirm the presence of distinct primary Fe(II) silicate minerals in the unaltered marine sediment core samples, we use an X-ray microprobe with a 2 μm × 2 μm X-ray beam size to identify and characterize individual Fe-rich particles in a glacial (42.7 ka) and interglacial (92.34 ka) sediment sample from the South Atlantic (Fig. 3). The small beam size allows us to probe the speciation of Fe in individual particles in the sediment sample (32), in contrast to bulk XAS, which provides the average Fe speciation and identifies the mix of minerals. Using μXRF maps, we observe large (~5 μm to 10 μm) Fe hotspots over a diffuse Fe signal representing most particles (*SI Appendix*, Fig. S9). We attribute these large hotspots to primary Fe minerals that are ground from bedrock, and we attribute the background to secondary Fe species (clays, Fe oxides) that are predominantly small (<2 μm) particles and aggregates (33–35). We use μXAS to determine the speciation and mineral composition of the hotspots; LCF at the near-edge region with standard spectra show that parts of these Fe hotspots are ~100% Fe(II) attributed solely to primary Fe(II) silicate minerals (biotite and hornblende were used as representative standards; Fig. 3). The particles in the glacial sediment are more reduced, on the whole, than those in the interglacial sediment (Fig. 3), and the Fe(II) hotspot/Fe$_{total}$ estimates from the μXRF maps (*SI Appendix*, Fig. S9) are nominally similar to the LCF-based Fe(II)/Fe$_{total}$ calculations (Fig. 2). Our identification of biotite- and hornblende-rich particles in the glacial and interglacial sediment provides evidence that distinct Fe(II) primary minerals are deposited to the Southern Ocean and preserved through the processes of sediment deposition, core collection, and core storage. We show evidence of pure Fe(II) silicates in both glacial and interglacial sediments (Fig. 3), which suggests glaciogenic minerals likely contribute to Fe(II)/Fe$_{total}$ throughout the glacial cycle, simply to a greater degree in glacial periods and to a lesser degree in interglacial periods.

We can rule out diagenetic controls on Fe speciation in the cores, because Fe(II) silicates dominate the Fe(II) signal. In marine sediments, the unknown impacts of diagenesis have precluded previous efforts to reconstruct dust-borne Fe speciation and bioavailability in the Southern Ocean over the last glacial cycle, since reducing conditions in the sediment can alter Fe oxidation state and speciation (36). Since primary Fe(II) silicates form only from cooling magma (37) and metamorphic processes above 500 °C (38, 39), changes in primary Fe(II) silicate concentrations represent glacial–interglacial changes in dust source [mainly the degree of physical weathering versus chemical weathering (31)] rather than diagenesis. Specifically, the primary Fe(II) silicates that are most commonly identified in sediments, including chlorite, biotite, and hornblende, cannot form under the low temperature and pressure conditions of sediment cores (37–39), and dominate glaciogenic dust sources impacted by physical weathering of bedrock (10, 11, 40). Secondary phyllosilicates (e.g., smectite, kaolinite, glauconite) produced during chemical weathering and diagenesis (41) can also contain some Fe(II), but they are structurally distinct from primary Fe(II) silicates (shown with biotite and glauconite XAS in Fig. 3) and represent minor contributions to the total Fe(II) signal except in interglacial periods [low dust, low Fe(II) content; *SI Appendix*, Fig. S8]. Iron sulfide minerals (e.g., pyrite, which was used in all LCF analyses), which would likely dominate any authigenic Fe(II) signal (36), contribute only minimally to the mineral composition of all samples as determined using LCF (*SI Appendix*, Fig. S8). However, sulfide minerals may not be well

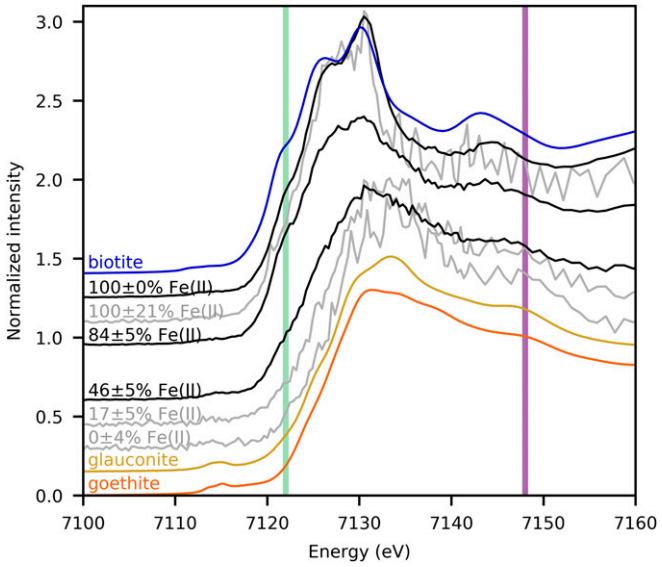

Fig. 3. Microprobe-based XAS of individual particles in a South Atlantic core (TN057-06), at a glacial and interglacial depth. The black solid lines are μXAS of three individual particles from the glacial sediment sample (42.7 ka), and the gray solid lines are μXAS of three individual particles from the interglacial sediment sample (92.34 ka). The spectra are labeled with their Fe(II)/Fe_{total} concentrations. Fe(II)/Fe_{total} was calculated using LCF of the sample with standards run contemporaneously, using the normalized intensity in the near-edge region (7,100 eV to 7,180 eV). The glacial particles were more reduced, on the whole, than the interglacial particles. A primary Fe(II) silicate standard (biotite, blue), an Fe(III) oxide/hydroxide standard (goethite, orange), and a secondary phyllosilicate standard (glauconite, goldenrod) are also plotted and labeled. The pure Fe(II) particles were >99% biotite and hornblende [primary Fe(II) silicates]. The vertical lines guide the eye to differences in edge positions (green) and postedge features (magenta) between the Fe(II) and Fe(III) rich samples. Spectra are offset for clarity.

preserved in storage under ambient air conditions. Iron carbonate is also minimal in all samples based on the LCF analysis. We thus expect that our Fe(II)/Fe_{total} values are lower-bound estimates but accurately represent changes in highly bioavailable primary Fe(II) silicate deposition to the subantarctic Southern Ocean on glacial–interglacial timescales.

We observe higher Fe(II) content [dominated by highly bioavailable glaciogenic Fe(II) silicates] in dust-borne Fe reaching the Southern Ocean during glacial periods versus interglacial periods. Thus, the speciation of Fe amplifies the impact of higher total Fe on the bioavailable Fe supply that increases phytoplankton productivity in the Southern Ocean in glacial periods.

The Impact of Glacial Activity and Fe Speciation on Bioavailable Fe Supply over the Last Glacial Cycle. When dust from modern sources is added to Fe-limited diatoms, diatom growth responds linearly to the particulate Fe(II) content (10). Thus, we suggest that Fe(II) flux is a more importance estimator of bioavailable Fe supply than total Fe flux. We use Fe supply amplification factors [Fe(II) flux and total Fe flux values from Fig. 2 for a given core at a given time point divided by the corresponding Holocene value] to determine the likely impact of Fe(II) versus total Fe on Fe fertilization over the last glacial cycle. Based on Fe(II) flux amplification factors for both the South Atlantic and South Pacific, there is consistently a ~15× to 20× higher bioavailable Fe supply to support phytoplankton growth in highly productive glacial periods compared with the current interglacial in both sectors of the Southern Ocean, and up to 30× higher bioavailable Fe supply in the South Atlantic during Marine Isotope Stage 3 between ~40 ka and 55 ka (Fig. 4). These Fe(II) flux amplification factors are at least 2× and up to 9× higher than corresponding total Fe flux amplification factors in all periods where dust flux is at a maxima and CO_2 is at a minima over the last glacial cycle (1) (Fig. 4), suggesting that Fe(II) fluxes are likely more important to Fe fertilization than total Fe fluxes throughout the Southern Ocean.

Our results show that glacial activity-driven changes in Fe speciation are positively correlated with dust flux and total Fe flux on glacial–interglacial timescales (*SI Appendix*, Fig. S4), suggesting that glacial activity is likely more important to both dust production and bioavailable Fe supply for a given dust/Fe flux than previously believed. We show that a given Fe flux is ~6× more bioavailable at the LGM compared with today, based on an increase in glaciogenic dust sources rich in highly bioavailable primary Fe(II) silicates. Thus, changes in Fe speciation are likely crucial to glacial Fe fertilization events in the Southern Ocean. Our observations are consistent with Antarctic ice core experiments demonstrating that dust-borne Fe is more soluble at the LGM than predicted by current models (13). Antarctic ice core LGM dust also supports persistent and relatively high dissolved Fe concentrations in diatom cultures (17), which could be explained by continuous dissolution of labile glaciogenic Fe(II) minerals. Our results suggest that Fe speciation should always be considered when evaluating the Fe supply and its impact on the biological pump. The tight correlation between Fe flux and Fe speciation (*SI Appendix*, Fig. S4) means that impacts of speciation may be misinterpreted as impacts of total Fe. Thus, the importance of Fe speciation on Fe fertilization of the Southern Ocean should be investigated further by looking for preserved molecular indicators of Fe nutrition in marine sediment cores and probing the impacts of dust-borne Fe speciation on bioavailable Fe supply in biogeochemical models.

The trends in Fe speciation over the last glacial cycle are remarkably similar between the subantarctic South Atlantic and South Pacific cores, which suggests there is a universal mechanism controlling the speciation and bioavailability of the dust sources in both of these regions. We show that Fe(II)/Fe_{total} reaches a minimum of ~5% to a maximum of ~45% across the full glacial cycle in both cores (Fig. 2), despite total Fe fluxes being ~3× lower in the South Pacific compared with the South Atlantic throughout the last glacial cycle. In sediments, primary Fe(II) minerals are characteristic of conditions of relatively high physical weathering, which mobilizes them from bedrock, and relatively low chemical weathering, which slows their transformation into secondary minerals (31). Clay mineral and quartz/feldspar ratios from the South Atlantic show that, compared with interglacial sediments, glacial sediments have undergone more physical weathering relative to chemical weathering (40). Given the link between modern glaciers and the primary Fe(II) content of dust sources (10), it is likely that physical glacial weathering influences the changes in dust-borne Fe speciation that we observe at high latitudes. Lower chemical weathering (drier climates) characteristic of glacial periods (44) could also contribute to higher Fe(II)/Fe_{total} in glacial periods, but some important South Atlantic and South Pacific dust sources experienced wetter conditions at the LGM (45, 46), so glacial weathering may be the dominant driver of Fe speciation on glacial–interglacial timescales. Despite the lower magnitude of dust fluxes in the South Pacific, which are thought to be dominated by Australian and New Zealand dust sources (8), the glacial–interglacial speciation changes are robust and similar to those in the South Atlantic, which are dominated by Patagonia dust sources (47, 48) that are highly impacted by glaciers (10). If glacial processes contributed significantly to high glacial Fe(II)/Fe_{total} in the South Pacific core, New Zealand may be a significant South Pacific dust source, as suggested by modern, modeled dust trajectories (49), since glacial activity was much more extensive at the LGM in New Zealand (50) versus Australia (51).

Our results suggest that dust sourced across the subantarctic Southern Ocean is more highly impacted by glacial activity at the LGM compared with today, which impacts its speciation and bioavailability. We show that glacial activity increases the highly bioavailable Fe(II) silicate content of dust reaching the Southern

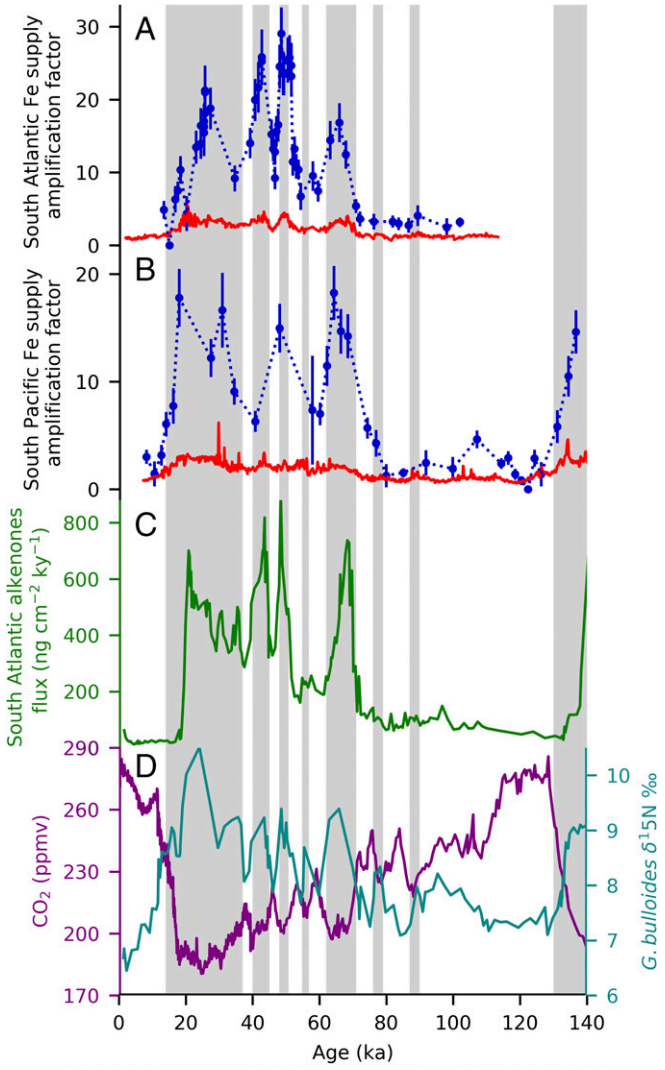

Fig. 4. Amplification factors for two measures of Fe supply [Fe flux in red solid lines and Fe(II) flux in blue circles connected with a dotted line] in (*A*) the South Atlantic (TN057-06) and (*B*) the South Pacific (PS75/56-1), with (*C*) alkenones and (*D*) atmospheric CO_2 and foraminifera-bound $\delta^{15}N$ records. (*A* and *B*) Amplification factors for Fe flux and Fe(II) flux show the relative increase from Holocene values, for each time point. Errors are propagated for Fe concentration, MAR, Fe(II)/Fe_{total} quantification, and the Holocene Fe(II) flux estimate. Dust flux maxima corresponding to atmospheric CO_2 minima in the last glacial cycle (1) are indicated in gray shaded bars in all plots, where Fe supply and productivity is high. In *C*, the alkenones flux (1, 42), a productivity proxy for the subantarctic South Atlantic core TN057-06/site OPD 1090, correlates with Fe supply over the last glacial cycle. In *D*, the *Globigerina bulloides* foraminifera-bound $\delta^{15}N$ record (1) from ODP 1090 (cyan solid line) and the atmospheric CO_2 record as recorded in Antarctic ice cores (43) (purple solid line) show the impacts of Fe fertilization over the last glacial cycle on surface nitrate utilization and climate, respectively.

Ocean, during periods of high total dust-borne Fe flux. This phenomenon is likely due to more mountain glaciers causing more physical weathering and more dust production in glacial outwash plains (52) at the LGM. We demonstrate that Fe(II) silicate-rich glacially derived Fe increases the bioavailable Fe supply by a factor of ∼15 to 20 in glacial versus interglacial periods, which is in comparison with the factor of ∼3 to 5 increases in total Fe flux that have been considered in biogeochemical models to date. Thus, the speciation of Fe should be included in models considering the importance of dust-borne Fe to Southern Ocean Fe fertilization. Our results suggest there is a positive feedback between glacial weathering and cold glacial temperatures, since glacial activity is associated with more bioavailable Fe for a given Fe flux. Thus, changes in the Fe speciation and bioavailability of dust sources are likely important drivers of glacial–interglacial changes in atmospheric CO_2 concentrations.

Materials and Methods

XAS Analysis for Bulk Sediments. Freeze-dried sediment samples were wrapped in metal-free and X-ray-transparent Kapton tape before being mounted in front of the X-ray beam. Iron K-edge X-ray absorption spectra were collected in fluorescence mode at the Stanford Synchrotron Radiation Lightsource (SSRL) beamlines 4-1 and 4-3 and the Advanced Photon Source beamline 10-BM, with 30-element Ge or passivated implanted planar silicon (PIPS), Lytle, and 4-element Si detectors, respectively. The Fe concentration of the marine sediment is between ∼0.5% and ∼2.5% Fe for all samples from TN057-06 (1) and PS75/56-1 (*SI Appendix*, Fig. S3), making them appropriate for XAS collected in fluorescence mode. All samples were run with the Fe foil standard in transmission mode, with the foil edge calibrated to 7,112.0 eV. The typical beam size is 1 mm by 10 mm. Spectral analysis was conducted with Matthew Newville's Larch Data Analysis Tools for X-ray Spectroscopy implemented in Python (25). Larch code and documentation is available at xraypy.github.io/xraylarch/. More details are available in *SI Appendix*, *Extended Materials and Methods: XAS Analysis for Bulk Sediments*.

Core Age Models and Proxy Data/Paleorecords. The two Southern Ocean sediment cores used in this study were TN057-06 from the subantarctic South Atlantic (9) and PS75/56-1 from the subantarctic South Pacific (8). The TN057-06 ^{230}Th-normalized ^{232}Th/dust flux (9), Fe flux (1), alkenones flux (42), and foraminifera-bound $\delta^{15}N$ data (1) are all previously published. The PS75/56-1 age model is from the supplement of the recently published Basak et al. (53). The PS75/56-1 ^{230}Th-normalized ^{232}Th/dust flux and Fe flux are published for the first time here, and were produced using established methods (21, 54). The Fe concentration was obtained from an XRF core scan (0.5-cm resolution) using an Avaatech XRF core scanner at the Alfred Wegener Institute for Polar and Marine Research. The Fe fluorescence counts were calibrated using >250 Fe concentration values from sediment digestions and inductively coupled plasma mass spectrometry (*SI Appendix*, Fig. S3). Analytical errors on ^{230}Th-normalized bulk mass accumulation rate (MAR) are 2%, and analytical error on Fe quantification is estimated at 5%. Errors are propagated as necessary, as described in the figure legends.

X-Ray Microprobe Analysis for Distinct Mineral Phases. We used the microprobe at SSRL beamline 2-3 (spot size 2 μm × 2 μm) to identify distinct mineral phases in unaltered South Atlantic (TN057-06) marine sediment core samples. Samples were mounted on a single sheet of Kapton tape, in a single layer of particles. We began with XRF maps to identify Fe hotspots, and collected XAS (in fluorescence mode with a Vortex Silicon Drift Detector) at the Fe K edge to determine the speciation of these Fe-rich particles. Spectral analysis was conducted with Larch (25). More details are available in *SI Appendix*, *Extended Materials and Methods: X-Ray Microprobe Analysis for Distinct Mineral Phases*.

Amplification Factor Calculations. Amplification factors for Fe supply [calculated separately for Fe(II) fluxes and total Fe fluxes for each core] are the Fe(II) or total Fe flux value at a given time point divided by the Holocene Fe(II) flux estimate or the average Holocene total Fe flux value, respectively, with error on the Holocene Fe(II) flux estimate approximated at 10%. The Holocene average for total Fe flux for both cores was the mean of all data points younger than 11.7 ka. The Holocene Fe(II) flux estimate for each core was the Holocene average total Fe flux multiplied by the best estimate of Holocene/interglacial Fe(II)/Fe_{total}. These best estimates were based on LCF-based Fe(II)/Fe_{total} values (Fig. 2 and *SI Appendix*, Fig. S2) and edge position data converted to Fe(II)/Fe_{total} (*SI Appendix*, Figs. S5 and S6). Data for all points younger than 11.7 ka were considered for TN057-06. Core PS75/56-1 has a longer Fe(II) record, so all points younger than 11.7 ka as well as points in the previous interglacial (119 ka to 124 ka) were considered. For both cores, the best estimates of Holocene/interglacial Fe(II)/Fe_{total} were ∼5%, and resulted in Fe(II) flux amplification factors that are ∼2× to 9× higher than total Fe flux amplification factors in all periods of dust maxima/CO_2 minima (1) over the last glacial cycle. If we use overly conservative Holocene Fe(II)/Fe_{total} values of ∼15%, based on some nonglaciogenic South American dust sources (10) that have higher Fe(II)/Fe_{total} than we observed in interglacial sediments in the cores, Fe(II) flux amplification factors are still ∼2× to 3× higher than total Fe flux amplification factors in most periods of dust maxima/CO_2 minima (1) over the last glacial cycle.

Statistical Analysis. For all LCF analysis, the error bars on the contribution from a given standard are produced by Larch (25) in the model of IFEFFIT (55), and are the diagonal elements of the covariance matrix, i.e., the variances of the individual components, when the reduced χ^2 has been corrected to be equal to 1. This correction is necessary because the estimate of measurement error used in the χ^2 calculation does not include sample inhomogeneity and detector nonlinearity, which are the dominant sources of measurement error in XAS collected from modern synchrotron light sources. When calculating $Fe(II)/Fe_{total}$ for each sediment sample, the LCF errors on the contribution from each standard are propagated, assuming a constant Fe(II) fraction for each standard.

Data Availability. All raw XAS data files and new PS75/56-1 data (^{232}Th flux and Fe flux) are deposited in the Columbia University Academic Commons, with the persistent URL: https://doi.org/10.7916/D8X07QHG.

ACKNOWLEDGMENTS. The authors acknowledge Satish C. B. Myneni and Michael R. Kaplan for discussions useful in refining the research, and Chandranath Basak for the PS75/56-1 age model from the supplement of Basak et al. (53). We thank Allison W. Jacobel for comments useful in editing the manuscript. This research used resources of the Advanced Photon Source, a US Department of Energy (DOE) Office of Science User Facility operated for the DOE Office of Science by Argonne National Laboratory under Contract DE-AC02-06CH11357. Use of the Stanford Synchrotron Radiation Lightsource, SLAC National Accelerator Laboratory, is supported by the US Department of Energy, Office of Science, Office of Basic Energy Sciences under Contract DE-AC02-76SF00515. E.M.S. is supported by National Science Foundation Graduate Research Fellowship DGE 16-44869. G.W. acknowledges support from National Science Foundation (NSF) Grant PLR-14-05204. B.C.B. acknowledges support by NSF Grant EAR-15-21356 and National Institute of Environmental Health Sciences Grant ES010349. This work is also supported by research funding from the Lamont-Doherty Earth Observatory Climate Center. This is Lamont contribution number 8257.

1. Martínez-García A, et al. (2014) Iron fertilization of the subantarctic ocean during the last ice age. *Science* 343:1347–1350.
2. Martínez-Garcia A, et al. (2011) Southern Ocean dust-climate coupling over the past four million years. *Nature* 476:312–315.
3. Jaccard SL, et al. (2013) Two modes of change in Southern Ocean productivity over the past million years. *Science* 339:1419–1423.
4. Sigman DM, Hain MP, Haug GH (2010) The polar ocean and glacial cycles in atmospheric $CO(_2)$ concentration. *Nature* 466:47–55.
5. Abelmann A, Gersonde R, Cortese G, Kuhn G, Smetacek V (2006) Extensive phytoplankton blooms in the Atlantic sector of the glacial Southern Ocean. *Paleoceanography* 21: PA1013.
6. Martínez-Garcia A, et al. (2009) Links between iron supply, marine productivity, sea surface temperature, and CO_2 over the last 1.1 Ma. *Paleoceanography* 24:PA1207.
7. Martin JH (1990) Glacial-interglacial CO_2 change: The iron hypothesis. *Paleoceanography* 5:1–13.
8. Lamy F, et al. (2014) Increased dust deposition in the Pacific Southern Ocean during glacial periods. *Science* 343:403–407.
9. Anderson RF, et al. (2014) Biological response to millennial variability of dust and nutrient supply in the subantarctic South Atlantic Ocean. *Philos Trans R Soc A* 372:20130054.
10. Shoenfelt EM, et al. (2017) High particulate iron(II) content in glacially sourced dusts enhances productivity of a model diatom. *Sci Adv* 3:e1700314.
11. Schroth AW, Crusius J, Sholkovitz ER, Bostick BC (2009) Iron solubility driven by speciation in dust sources to the ocean. *Nat Geosci* 2:337–340.
12. Hawkings JR, et al. (2018) Biolabile ferrous iron bearing nanoparticles in glacial sediments. *Earth Planet Sci Lett* 493:92–101.
13. Conway TM, Wolff EW, Röthlisberger R, Mulvaney R, Elderfield HE (2015) Constraints on soluble aerosol iron flux to the Southern Ocean at the Last Glacial Maximum. *Nat Commun* 6:7850.
14. Edwards R, Sedwick P, Morgan V, Boutron C (2006) Iron in ice cores from Law Dome: A record of atmospheric iron deposition for maritime East Antarctica during the Holocene and Last Glacial Maximum. *Geochem Geophys Geosyst* 7:Q12Q01.
15. Spolaor A, et al. (2013) Iron speciation in aerosol dust influences iron bioavailability over glacial-interglacial timescales. *Geophys Res Lett* 40:1618–1623.
16. von der Heyden BP, Roychoudhury AN, Mtshali TN, Tyliszczak T, Myneni SCB (2012) Chemically and geographically distinct solid-phase iron pools in the Southern Ocean. *Science* 338:1199–1201.
17. Conway TM, Hoffmann LJ, Breitbarth E, Strzepek RF, Wolff EW (2016) The growth response of two diatom species to atmospheric dust from the Last Glacial Maximum. *PLoS One* 11:e0158553.
18. Tagliabue A, et al. (2016) How well do global ocean biogeochemistry models simulate dissolved iron distributions? *Global Biogeochem Cycles* 30:149–174.
19. Mahowald NM, et al. (2006) Change in atmospheric mineral aerosols in response to climate: Last glacial period, preindustrial, modern, and doubled carbon dioxide climates. *J Geophys Res Atmos* 111:D10202.
20. Gersonde R, Hodell DA, Blum P (1999) *Proceedings of the Integrated Ocean Drilling Program: Initial Report* (Ocean Drill Program, College Station, TX), Vol 177.
21. Winckler G, Anderson RF, Fleisher MQ, McGee D, Mahowald N (2008) Covariant glacial-interglacial dust fluxes in the equatorial Pacific and Antarctica. *Science* 320:93–96.
22. Anderson RF, et al. (2016) How well can we quantify dust deposition to the ocean? *Philos Trans A Math Phys Eng Sci* 374:20150285.
23. Taylor SR, McLennan SM (1985) *The Continental Crust: Its Composition and Evolution* (Blackwell Scientific, Oxford).
24. McGee D, Marcantonio F, Lynch-Stieglitz J (2007) Deglacial changes in dust flux in the eastern equatorial Pacific. *Earth Planet Sci Lett* 257:215–230.
25. Newville M (2013) Larch: An analysis package for XAFS and related spectroscopies. *J Phys Conf Ser* 430:012007.
26. Formenti P, et al. (2014) Dominance of goethite over hematite in iron oxides of mineral dust from Western Africa: Quantitative partitioning by X-ray absorption spectroscopy. *J Geophys Res Atmos* 119:12740–12754.
27. Lisiecki LE, Raymo ME (2005) A Pliocene-Pleistocene stack of 57 globally distributed benthic $d^{18}O$ records. *Paleoceanography* 20:PA1003.
28. Raymo ME (1994) The initiation of Northern Hemisphere glaciation. *Annu Rev Earth Planet Sci* 22:353–383.
29. Lambert F, Bigler M, Steffensen JP, Hutterli M, Fisher H (2012) Centennial mineral dust variability in high-resolution ice core data from Dome C, Antarctica. *Clim Past* 8: 609–623.
30. Ingall ED, et al. (2013) Role of biogenic silica in the removal of iron from the Antarctic seas. *Nat Commun* 4:1981.
31. Sposito G (2008) *The Chemistry of Soils* (Oxford Univ Press, New York).
32. Marcelli A, et al. (2012) XRF-XANES characterization of deep ice core insoluble dust. *J Anal At Spectrom* 23:33–37.
33. Brindley GW, Brown G (1980) *Crystal Structures of Clay Minerals and Their X-Ray Identification* (Mineral Soc, London).
34. Cornell RM, Schwertmann U (2003) *The Iron Oxides: Structure, Properties, Reactions, Occurences and Uses* (Wiley, Weinheim, Germany), 2nd Ed.
35. Journet E, Balkanski Y, Harrison SP (2014) A new data set of soil mineralogy for dust-cycle modeling. *Atmos Chem Phys* 14:3801–3816.
36. Schulz HD, Dahmke A, Schinzel U, Wallmann K, Zabel M (1994) Early diagenetic processes, fluxes, and reaction rates in sediments of the South Atlantic. *Geochim Cosmochim Acta* 58:2041–2060.
37. Bowen NL (1922) The behavior of inclusions in igneous magmas. *J Geol* 30(Suppl): 513–570.
38. Bushmin SA, Glebovitsky VA (2008) Scheme of mineral facies of metamorphic rocks. *Geol Ore Deposits* 50:659–669.
39. Eskola P (1920) The mineral facies of rocks. *Nor Geol Tidsskr* 6:143–194.
40. Diekmann B, Kuhn G (2002) Sedimentary record of the mid-Pleistocene climate transition in the southeastern South Atlantic (ODP Site 1090). *Palaeogeogr Palaeoclimatol Palaeoecol* 182:241–258.
41. Baldermann A, Warr LN, Letofsky-Papst I, Mavromatis V (2015) Substantial iron sequestration during green-clay authigenesis in modern deep-sea sediments. *Nat Geosci* 8:885–890.
42. Sachs JP, Anderson RF (2003) Fidelity of alkenone paleotemperatures in southern Cape Basin sediment drifts. *Paleoceanography* 18:PA1082.
43. Lüthi D, et al. (2008) High-resolution carbon dioxide concentration record 650,000-800,000 years before present. *Nature* 453:379–382.
44. Rea DK (1994) The paleoclimatic record provided by eolian deposition in the deep sea: The geologic history of wind. *Rev Geophys* 32:159–195.
45. Kohfeld KE, et al. (2013) Southern Hemisphere westerly wind changes during the Last Glacial Maximum: Paleo-data synthesis. *Quat Sci Rev* 68:76–95.
46. McGee D, Broecker WS, Winckler G (2010) Gustiness: The driver of glacial dustiness? *Quat Sci Rev* 29:2340–2350.
47. Gili S, et al. (2016) Provenance of dust to Antarctica: A lead isotopic perspective. *Geophys Res Lett* 43:2291–2298.
48. Delmonte B, et al. (2004) Comparing the EPICA and Vostok dust records during the last 220,000 years: Stratigraphical correlation and provenance in glacial periods. *Earth Sci Rev* 66:63–87.
49. Neff PD, Bertler NAN (2015) Trajectory modeling of modern dust transport to the Southern Ocean and Antarctica. *J Geophys Res Atmos* 120:9303–9322.
50. Barrell DJA (2011) Quaternary glaciers of New Zealand. *Developments in Quaternary Science*, eds Ehlers J, Gibbard P, Hughes P (Elsevier, Amsterdam), Vol 15, pp 1047–1064.
51. Barrows TT, Stone JO, Fifield LK, Cresswell RG (2001) Late Pleistocene glaciation of the Kosciuszko Massif, Snowy Mountains, Australia. *Quat Res* 55:179–189.
52. Sugden DE, McCulloch RD, Bory AJ-M, Hein AS (2009) Influence of Patagonian glaciers on Antarctic dust deposition during the last glacial period. *Nat Geosci* 2:281–285.
53. Basak C, et al. (2018) Breakup of last glacial deep stratification in the South Pacific. *Science* 359:900–904.
54. Fleisher MQ, Anderson RF (2003) Assessing the collection efficiency of Ross Sea sediment traps using ^{230}Th and ^{231}Pa. *Deep Sea Res Part II* 50:693–712.
55. Newville M (2001) IFEFFIT: Interactive XAFS analysis and FEFF fitting. *J Synchrotron Radiat* 8:322–324.